Device

Article

Peltier cooling for thermal management in nanofluidic devices

Graphical abstract

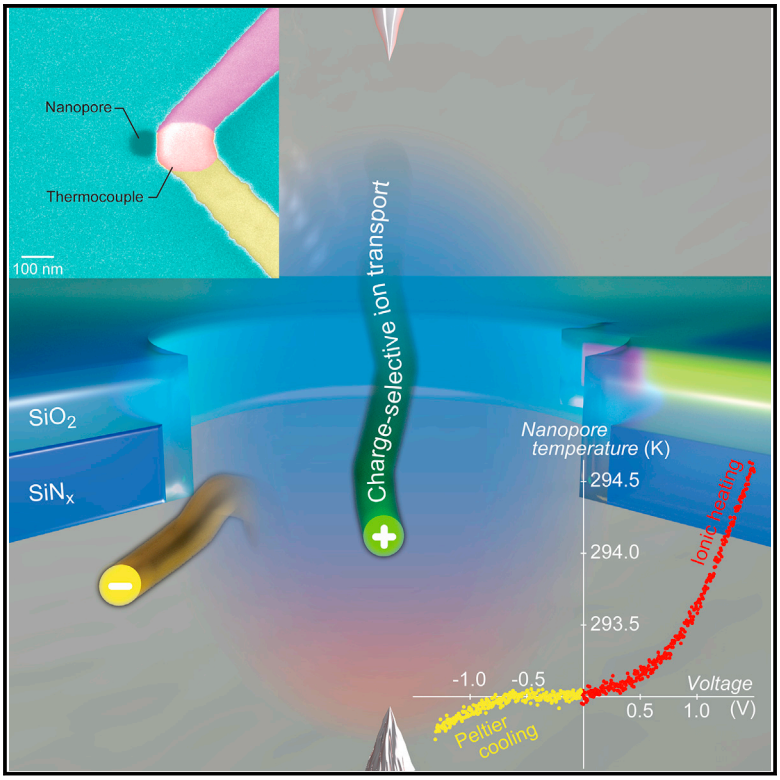

Highlights

- Spot-cooling nanopore device can be created based on charge-selective ion transport
- Demonstration using a SiO_2/SiN_x membrane nanopore in a NaCl solution of various salinity
- Proof-of-concept device achieved an ionic cooling efficiency of −0.2 K/nW

Authors

Makusu Tsutsui, Kazumichi Yokota, Wei Lun Hsu, Denis Garoli, Hirofumi Daiguji, Tomoji Kawai

Correspondence

tsutsui@sanken.osaka-u.ac.jp (M.T.), kawai@sanken.osaka-u.ac.jp (T.K.)

In brief

The charge selectivity of a nanopore for ion transport also causes local cooling analogous to the Peltier cooling effect found in semiconductors. The authors present the theoretical framework and experimental observations of Peltier cooling in a nanopore. The temperature of a nanopore can be increased or decreased by the electric field-driven ion flow depending on the ionic strength conditions. The heating/cooling transition occurred when the Dukhin length became longer than the nanopore diameter, where the charge-selectivity dominates the counter-cation conduction.

Understand
Early stage research on device properties, design, and physics

Tsutsui et al., 2023, Device *1*, 100188
December 22, 2023 Published by Elsevier Inc.
https://doi.org/10.1016/j.device.2023.100188

CellPress

Please cite this article in press as: Tsutsui et al., Peltier cooling for thermal management in nanofluidic devices, Device (2023), https://doi.org/10.1016/j.device.2023.100188

Device

CellPress
OPEN ACCESS

Article

Peltier cooling for thermal management in nanofluidic devices

Makusu Tsutsui,[1,5,*] Kazumichi Yokota,[2] Wei Lun Hsu,[3] Denis Garoli,[4] Hirofumi Daiguji,[3] and Tomoji Kawai[1,*]
[1]The Institute of Scientific and Industrial Research, Osaka University, 8-1 Mihogaoka, Ibaraki, Osaka 5267-0047, Japan
[2]National Institute of Advanced Industrial Science and Technology, Takamatsu, Kagawa 761-0395, Japan
[3]Department of Mechanical Engineering, The University of Tokyo, 7-3-1, Hongo, Bunkyo-ku, Tokyo 113-8656, Japan
[4]Instituto Italiano di Tecnologia, Optoelectronics Research Line, Morego 30, 16163 Genova, Italy
[5]Lead contact
*Correspondence: tsutsui@sanken.osaka-u.ac.jp (M.T.), kawai@sanken.osaka-u.ac.jp (T.K.)
https://doi.org/10.1016/j.device.2023.100188

THE BIGGER PICTURE Thermodynamics at the nanoscale can be very different from macroscopic systems because certain heating/cooling effects can play a much larger role. We report on observations of Peltier cooling in a nanopore analogous to that observed in semiconductors. We discovered that the temperature of the nanopore can be adjusted either up or down by using an electric field to drive the flow of ions, depending on the concentration of the ions present. The transition between heating and cooling happens when the Dukhin length becomes greater than the diameter of the nanopore. This change indicates that the counter-cation conduction at the pore wall plays a significant role in the local cooling of the nanopore. The findings have implications for a wide range of systems, from designing the thermal management of nanofluidic osmotic power generators, to understanding the temperature regulation mechanism in ion channels of living cells.

SUMMARY

Permselectivity is a fundamental property of ion channels that enables one-way flow of specific cations or anions through cell membranes. Although energy dissipation phenomena in these ion channels involving thermoelectricity have been thoroughly investigated, heat transport for these channels at the nanoscale remains relatively unexplored. Here we report on nanofluidic thermoelectric cooling via the Peltier effect driven by charge-selective ion transport. We discovered that, when the ion concentration was high, the local temperature increased with the input electrical power via non-selective ion flow-mediated heat dissipation. In contrast, the nanopore temperature decreased with increasing transmembrane voltage in low-salinity water, where the negative surface charges at the channel wall rendered cation selectivity to allow heat pumping via the counter-ion flux. This ionic refrigeration may be used for thermal management in nanofluidic devices and shows insights into temperature regulation mechanisms within ion channels of live cells.

INTRODUCTION

Electrically driven ion flow in an isothermal nanopore involves collisions with water molecules that induce local heating analogous to Joule heating by electron conduction in a solid-state matter.[1–4] While the ionic heat dissipates through the aqueous media by convection and conduction, ions themselves also carry heat as they move along the electric field.[5,6] The associated heat transport is predicted as isotropic in macroscopic channels due to the equal contributions of cations and anions flowing in opposite directions under transmembrane voltage. In contrast, the fluidic channel becomes permselective as its diameter reaches a lower limit.[7,8] For instance, biological pores in transmembrane proteins are capable of gating the transport of specific ions via the ingenious molecular mechanism.[9,10] Solid-state nanopores can implement charge-selectivity by exploiting the electrostatic repulsions at the wall surface charges to admit only cations or anions to pass through the nano-confined space.[7,11] The resulting ion flow generates electric potential difference under a temperature gradient,[12] allowing various functions such as thermosensation in living organisms[13] and thermoelectric energy conversions for blue energy harvesting.[14] There may also be a way to reverse engineer the phenomenon of ionic heat pump to enable nanopore refrigeration (i.e., Peltier cooling using ion-selective transport),[15] which can be used for thermal management at the nanoscale. Such a function can be used to control heat dissipation in nanoporous membrane osmotic power generators and integrated iontronic

Please cite this article in press as: Tsutsui et al., Peltier cooling for thermal management in nanofluidic devices, Device (2023), https://doi.org/10.1016/j.device.2023.100188

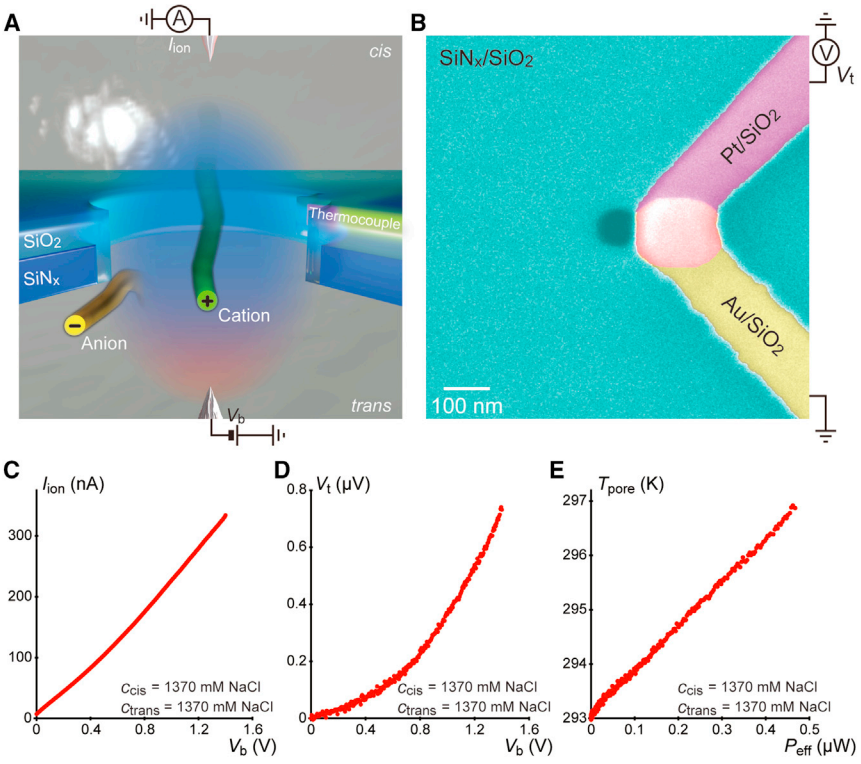

Figure 1. Measurements of local ionic energy dissipation at nanopores

(A) Schematic of the measurement configuration. The ionic current I_{ion} through the nanopore in electrolyte buffers was measured under the applied transmembrane voltage V_b. The voltage V_t at the embedded nanowire thermocouple was monitored to evaluate the influence of the ion transport on the local temperature.

(B) SEM image of a thermocouple-embedded nanopore. The Au and Pt nanowires formed a point contact near the 50-nm-sized nanopore, which served as a thermocouple. The nanowires were coated with a thin SiO_2 layer to avoid cross-talk with V_b.

(C) The ionic current versus transmembrane voltage characteristics of the nanopore in 1.37 M NaCl.

(D) The thermovoltage at the thermocouple.

(E) The nanopore temperature T_{pore} deduced from V_t in (D). The linear increase in T_{pore} with the input electric power $P_{eff} = I_{ion}V_b$ indicates nanopore temperature increase by ionic Joule heating.

circuits, where ionic heating from higher ion flux density poses a technological bottleneck.

RESULTS

Experimental set up of the thermocouple-embedded nanopore

We created a junction of Au and Pt nanowires in the form of a thermocouple to address the thermoelectricity-mediated energy transport in an ion-carrying nanopore with a 50-nm diameter in a dielectric membrane of 50-nm thickness (Figures 1A and 1B). The ionic current (I_{ion}) through the pore and the thermovoltage (V_t) at the thermocouple were simultaneously measured under ramps of the transmembrane voltage (V_b) in PBS containing NaCl (salt) at various concentrations (pH is 7.4 unless stated otherwise) (Figures S1 and S2). When the salt concentrations on both the *cis* (c_{cis}) and *trans* (c_{trans}) sides of the pore were the same at 1.37 M (Figure 1C), the $I_{ion} - V_b$ characteristics were linear with the ionic conductance G_{pore} of 213 nS fairly agreeing with the Maxwell-Hall's expression[16] $G_{pore} = \sigma(1/d_{pore} + 4L_{mem}/\pi d_{pore}^2)^{-1}$ within 4%, where $\sigma = 10$ S/m is the conductivity of the electrolyte buffer, d_{pore} (=50 nm) is the pore diameter, and L_{mem} (= 50 nm) is the thickness of the membrane. This result indicates diffusive transport of ions under negligible influence of the negative surface charges at the pore wall due to screening of the electrostatic potential in the high-ionic-strength solution (Debye length λ_{Debye} is 0.26 nm at 1.37 M NaCl).[17] Because the electromigration of ions involves energy dissipation as they collide with water molecules, the associated Joule heating raises the local temperature T_{pore} at the nanopore,[1–4] which is sensed by the thermocouple as a rise in V_t (Figure 1D) (calibrated to change with T_{pore} as $V_t = 1.7 \times 10^{-7}\ T_{pore}$).[4] Under such a condition, the nanopore is a simple resistive heater with its temperature increasing linearly with the input electric power $P_{in} = I_{ion}V_b$ at the same rates under different voltage directions (Figure S3) signifying the steady-state energy flow under the balance between the ionic heating and the associated heat transfer by ions and water convection (Figure 1E).[18,19]

Observed ionic refrigeration in ion-selective nanopores

Asymmetry can be induced in the ionic current characteristics by a salinity difference across the membrane (Figure 2).[20] Reducing the salt concentration at the *cis*, I_{ion} showed rectifying behaviors under negative V_b, which is attributed to two distinct mechanisms: electroosmosis-driven ion concentration modulations[21] and cation-selective transport in the synthetic nanopore with negative charges at the wall surface[22] (shown in Figures 2A and 2D, where the ionic current is plotted as a function of the effective voltage $V_{eff} = V_b - V_{ele}$, where V_{ele} is the redox potential at the electrodes under the salinity conditions tested[23]). The electroosmosis-driven ion concentration modulations arise from the electroosmotic flow at the negatively charged wall[24] that pumps the saline water into the pore, varying the local oluteion conductivity in a V_b-dependent manner.[21] Meanwhile, the cation-selective transport stems from the charge selectivity of the nanopore due to the electrostatic repulsion of anions by the surface charge of the membrane that brings higher or lower flows of cations depending on the polarity of the voltage.[22] These two distinct mechanisms yielded more pronounced diode-like characteristics under larger salt gradients (Figures S3–S10). Relatively smaller power is dissipated under negative V_b demonstrating asymmetry in the $T_{pore} - P_{eff}$ characteristics, where $P_{eff} = I_{ion}(V_b - V_{ele})$ is the effective power dissipated at the nanopore.

Please cite this article in press as: Tsutsui et al., Peltier cooling for thermal management in nanofluidic devices, Device (2023), https://doi.org/10.1016/j.device.2023.100188

CellPress
OPEN ACCESS

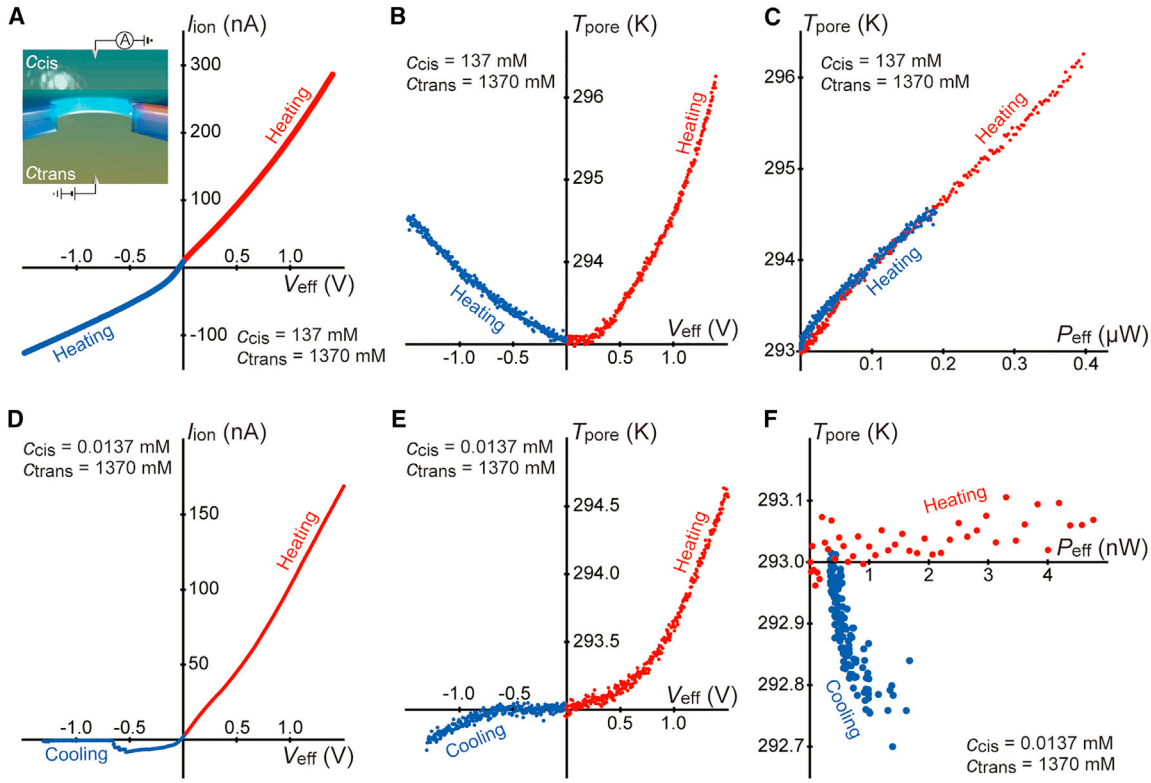

Figure 2. Ionic cooling of nanopores

(A and B) The ionic current (A) and nanopore temperature changes (B) against the transmembrane voltage under a 10-fold salinity difference (*cis*: 137 mM; *trans*: 1370 mM) across the membrane. Red and blue plots denote the data at positive and negative transmembrane voltage $V_b - V_{ele}$, respectively, where V_{ele} is the redox potential.

(C) T_{pore} plotted as a function of P_{eff} indicating the temperature increase by ionic heating irrespective of voltage polarity.

(D–F) Results under 10^5-fold salinity difference (*cis*: 0.0137 mM; *trans*: 1370 mM) demonstrating nanopore refrigeration at negative V_b.

Yet, the rates of temperature change $\alpha = T_{pore}/P_{eff}$ are found to be almost the same regardless of the voltage polarity at moderate salinity difference of r_{salt} ($=c_{trans}/c_{cis}$) $\leq$ 1,000 (see Figures 2B, 2C, and S3–S5) for the amount of heat generated per field-accelerated ions, and the dissipation efficiency through water also remain unaltered. At $r_{salt} \geq$ 10,000, in contrast, the ion transport caused refrigeration. The nanopore temperature increased at a constant rate of around 7 K/μW under positive V_b, T_{pore}, but decreased below the ambient at a rate up to −208 K/μW under negative voltages (see Figures 2E, 2F, and S6–S8).

This electrical cooling phenomenon is ascribable to the ionic thermoelectricity in the permselective nanopore. The negative native charges at the dielectric surface in the buffer[24] electrostatically attract cations to the channel wall. The dense counterions become the major carriers in dilute electrolyte solution, giving rise to the cation-selective transport in the nanopore. As ions carry heat,[5,6] the electromigration of the dense counterions is expected to induce temperature difference across the nanopore analogous to the Peltier effect in a semiconductor, thereby leading to the refrigeration when the ionic cooling is more effective than the Joule heating. Dukhin length (L_D) characterizes the contribution of this surface conduction mechanism, which becomes significant when $d_{pore} < L_D = \sigma_{wall}/2ec_{ion}$, where σ_{wall}, e, and c_{ion} are the pore wall surface charge density, the elementary charge, and the salt concentration, respectively.[25,26] Diluter salt solution, therefore, anticipates more prominent cooling with V_b, which is seen as smaller α at lower c_{cis} (Figure 3A). Quantitatively, L_D is about 57 nm at c_{ion} = 1.37 mM and σ_{wall}[24] = −15 mC/m^2 predicting the non-selective nature of the in-pore ion transport,[25] and hence ineffective ionic cooling, at $r_{salt} \leq$ 1,000. Under these salinity conditions, we observed nanopore Joule heating irrespective of the direction of the transmembrane voltage. Meanwhile, the Dukhin length becomes much longer than d_{pore} with $c_{ion} \leq$ 0.137 mM ($L_D \geq$ 570 nm), thus enabled to decrease T_{pore} to below the surrounding temperature by the pronounced ionic Peltier effect (Figure 3B).

We note the indirect role of electroosmosis on the energy dissipation in the nanofluidic channel. Negative V_b generates *cis*-to-*trans* electroosmotic flow that pushes the low-salt-concentration solution into the nanopore.[21] The depleted ion density leads to the ionic current rectification, as also observed in the finite element simulations (Figure 3C). At the same time, the dilute ion concentration enhances the counterion effect[25,26] to allow the nanopore cooling. The water flows in an opposite direction under positive voltage serving to enrich ions in the channel. In this case, no notable contribution of the surface conduction is

Please cite this article in press as: Tsutsui et al., Peltier cooling for thermal management in nanofluidic devices, Device (2023), https://doi.org/10.1016/j.device.2023.100188

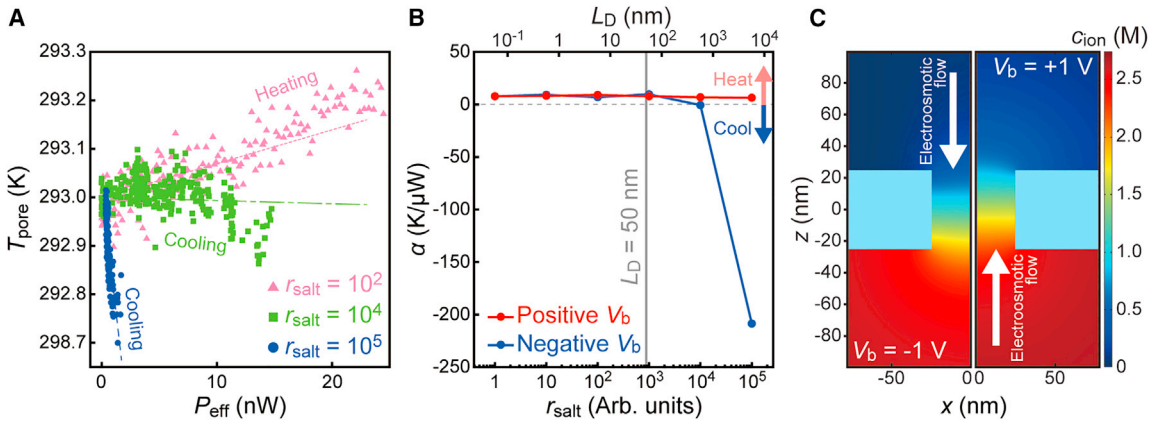

Figure 3. Nanopore cooling efficiency

(A) $T_{pore} - P_{eff}$ plots under various ion concentration ratio $r_{salt} = c_{trans}/c_{cis}$ across the membrane. Dashed lines are linear fits to the data. The slopes α denote the efficiencies of the ionic heating/cooling under the ionic conditions tested.

(B) α as a function of r_{salt} and the Dukhin length L_D. Dashed line denotes $\alpha = 0$. Gray line points at $L_D = 50$ nm. Cooling effects were observed for $L_D < d_{pore}$ when $r_{salt} \geq 10^4$.

(C) Salt concentration distributions around a nanopore at $r_{salt} = 10^3$ under −1 V (left) and +1 V (right) obtained by finite element simulations. The electroosmotic flow pushes the high- and low-ion concentration water into the nanopore in a voltage polarity dependent manner. The high ionic strength at positive voltages brings weak charge-selectivity of the nanopore via Debye screening and weakens the counterion transport-mediated heat pumping. On the contrary, the pore is filled with more dilute salt solution under negative V_b that leads to enhanced cation selectivity and more pronounced ionic Peltier cooling.

expected giving rise to the increase in T_{pore} by the ionic heat dissipation.[4]

The nanopore cooling was confirmed as reversible upon changing the direction of V_b scans (Figure S11). Changing the transmembrane voltage slowly from −1.0 to −1.5 V at a rate of around 12 mV/s, T_{pore} decreased steadily below the room temperature. Reversing the scanning direction resulted in a gradual increase in the nanopore temperature upon returning V_b from −1.5 V to −1.0 V. The $V_b - T_{pore}$ plots were completely the same during the two processes without any transient behaviors suggesting the steady-state change of the nanopore temperature via the ionic cooling.

The effect of permselectivity on the ionic cooling

The importance of the ion selectivity on the local ionic cooling was verified by examining the T_{pore} measurements in alkaline solutions. The $I_{ion} - V_b$ curves at r_{salt} of 10^5 displayed larger short circuit current upon increasing pH from 7 to 11 (Figure 4A; see also Figures S12 and S13). It suggests stronger cation-selective transport in the more basic liquids as they provide higher charge densities at the pore wall surface.[11,27] Accordingly, nanopore cooling behaviors were found as more evident in alkaline pH (Figure 4B).

The efficacy of the ionic cooling was further examined with a micrometer-scale channel. Although the counterion transport gives negligible contribution to the transmembrane ion flow, the electroosmotic pumping mechanism[21] led to clear I_{ion} rectification characteristics in a 3-μm-diameter pore under r_{salt} of 10^5 (Figures S14–S17).[21] Nevertheless, unlike the case for the nanopores, T_{pore} increased at both positive and negative transmembrane voltages without showing signs of the Peltier cooling partly due to the relatively high ion concentration in this micropore that makes $d_{pore} > L_D$ (Figure S15). The result corroborates the role of the ion selectivity on the nanopore refrigeration.

Local cooling is anticipated to occur without a salt gradient. To confirm this, we carried out the T_{pore} measurements of a 50-nm-sized nanopore without salinity difference. The $I_{ion} - V_b$ characteristics revealed weak rectification behaviors upon decreasing c_{cis} and c_{trans} down to 0.137 mM (Figure 4C; see also Figures S18 and S19) due presumably to the charge asymmetry in the SiO_2-covered SiN_x membrane surfaces making the top layer more negatively charged in the electrolyte buffer.[28] As expected, nanopore refrigeration was observed in dilute salt solutions satisfying $d_{pore} < L_D$ with enhanced cooling efficiency at lower ionic strengths (Figure 4D; see also Figures S17 and S18).

The present results are consistent to support the influence of ionic thermoelectricity in charge-selective nanofluidic channels. We detected increasing open circuit voltage V_{therm} upon imposing larger temperature difference ΔT across the membrane with a 50-nm-diameter pore at c_{ion} = 0.137 mM (Figure 5A).[12] The sign of the thermovoltage was found to be negative, which suggested cation-selective transport via thermal diffusion.[11] This was not the case for a micropore, where the V_{therm} remained low under the applied thermal gradients due to the absence of charge-selectivity along with the little difference in the Soret coefficients[29] of Na^+ and Cl^-, as well as the relatively small thermogalvanic effect for the electrochemical reactions at the Ag/AgCl electrodes[30] (Figure S20). The observation of the thermoelectric voltage in the cation-selective nanopore, therefore, anticipates the contribution from the reverse phenomenon of Peltier cooling under bias voltage.

The linear dependence of V_{therm} on ΔT gives the thermopower S (= $-V_{therm}/\Delta T$) of 3.5 mV/K, from which the Peltier coefficient Π (= ST) of around 1.0 V is deduced at the environmental temperature T of 293 K (Figure 5B).[31,32] With this Π, the thermoelectric transport in the nanopore is simulated at 0.137 mM NaCl by solving Poisson-Nernst-Plank and Navier-Stokes equations in a

Please cite this article in press as: Tsutsui et al., Peltier cooling for thermal management in nanofluidic devices, Device (2023), https://doi.org/10.1016/j.device.2023.100188

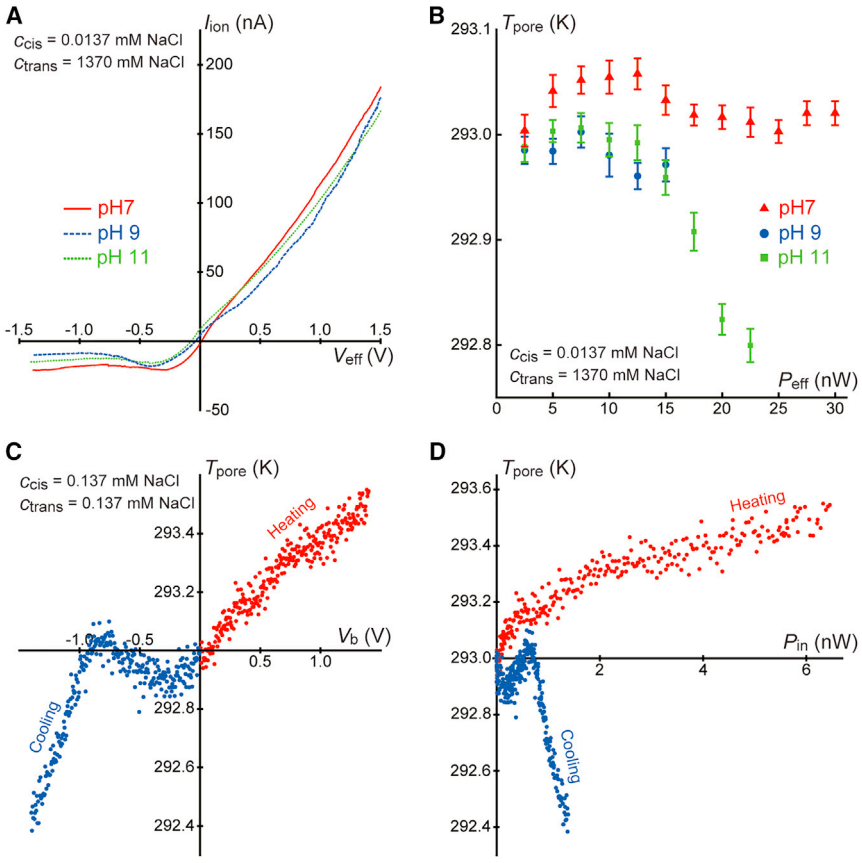

Figure 4. Nanopore refrigeration under various conditions

(A) pH dependence of the ionic current characteristics of a 50 nm-sized nanopore under 10^5-fold salinity difference. The larger negative open circuit voltage at higher pH from 7 to 11 indicates stronger charge-selectivity due to larger surface charge densities at nanopore wall surface in more alkaline environments.

(B) T_{pore} – P_{eff} characteristics exhibiting more pronounced nanopore cooling under higher pH. Error bars denote the standard deviations in the nanopore temperatures measured three times.

(C) Nanopore temperature in a dilute electrolyte solution without salinity difference demonstrating Peltier cooling effects at negative V_b.

(D) T_{pore} in (c) plotted as a function of P_{eff}. Color coding is the same as that in (C).

framework of a finite element method.[2,4] It revealed the thermal flux near the wall surface stemming from the heat transport via the voltage-driven counter-cations under $V_b = \pm 1$ V (Figures 5C and 5D). Moreover, being a counterion effect, the Peltier cooling can be made more efficient by enlarging the nanopore surface charge density (Figure 5E), thereby enabling thermal management at nanoscale.

DISCUSSION

By exploiting the Peltier cooling effect, thermoelectric refrigeration can be realized by charge-selective ion flow in a nanopore for spot-cooling at the nanoscale space. The cooling nanopores can be scaled up by extending the nanofluidic channel into multipore arrays. It would also be compatible with nanopipette techniques to enable a thermoelectric probe for scanning and manipulating the local temperature at nanoscale in liquid. To guide future efforts, there is room to refine the structure and material designs for more efficient and precise temperature control, and to explore how these nanopores can be integrated in real world devices.

Considerations for the ionic cooling efficiency

The electromigration of counter-cations may involve dehydration, the process of which anticipates nanopore cooling via heat consumption upon the disruption of the hydrogen bonds. Nevertheless, the ion dehydration is primarily driven by the steric effect. Previous work on dehydration of sodium ions in nanochannels focused on cases where the channel sizes are close to their hydrated radius.[33] For larger channels, a prior molecular dynamics study on electroosmosis in a single-digit nanochannel, which is one order of magnitude smaller than the nanopores studied here, shows that the dehydration of potassium ions, whose hydrated radius is approximately 3.7 Å, only appears within 5 Å near the channel wall.[34] Away from this region, the hydration number of ions is close to the saturation value, despite the application of an external electric field an order of magnitude higher than that in our experimental system. Furthermore, the dehydration free energy of sodium ions, 388 kJ/mol,[35] is much higher than the enthalpy of vaporization (44 kJ/mol) and hydrogen bond enthalpy of water molecules (23.3 kJ/mol), making it difficult for dehydration of ions to be triggered by an external electric field or local heating. Therefore, it is less likely that ion dehydration played a notable role on the energy dissipation in the ion-carrying 50-nm-sized nanopore.

The ionic cooling efficiency is expected to vary by nanopore geometries. In principle, the rate of heat carried by the counterion transport is anticipated to be given by the product of the ionic current and the Peltier coefficient.[15] The Peltier coefficient is expected to be proportional to the Seebeck coefficient, which is determined by the ion selectivity in the nanopore for the given ion species and their concentration in the fluid. In this regard, nanopores smaller than 50 nm persist to be charge-selective in higher ionic strength solutions allowing to leverage the stronger heat transfer via the enriched counterions at the pore wall surface. At the same time, the volume of water, and equivalently the heat capacity, relevant to the energy dissipation becomes smaller. The overall changes anticipate more efficient temperature control via the ionic refrigeration in smaller nanopores. Meanwhile, making the pores longer than 50 nm would benefit from the more prominent surface charge effects to render stronger ion selectivity[7]; however, pores that are too long would lower the ionic conductance[36] and impair the cooling efficiency by the

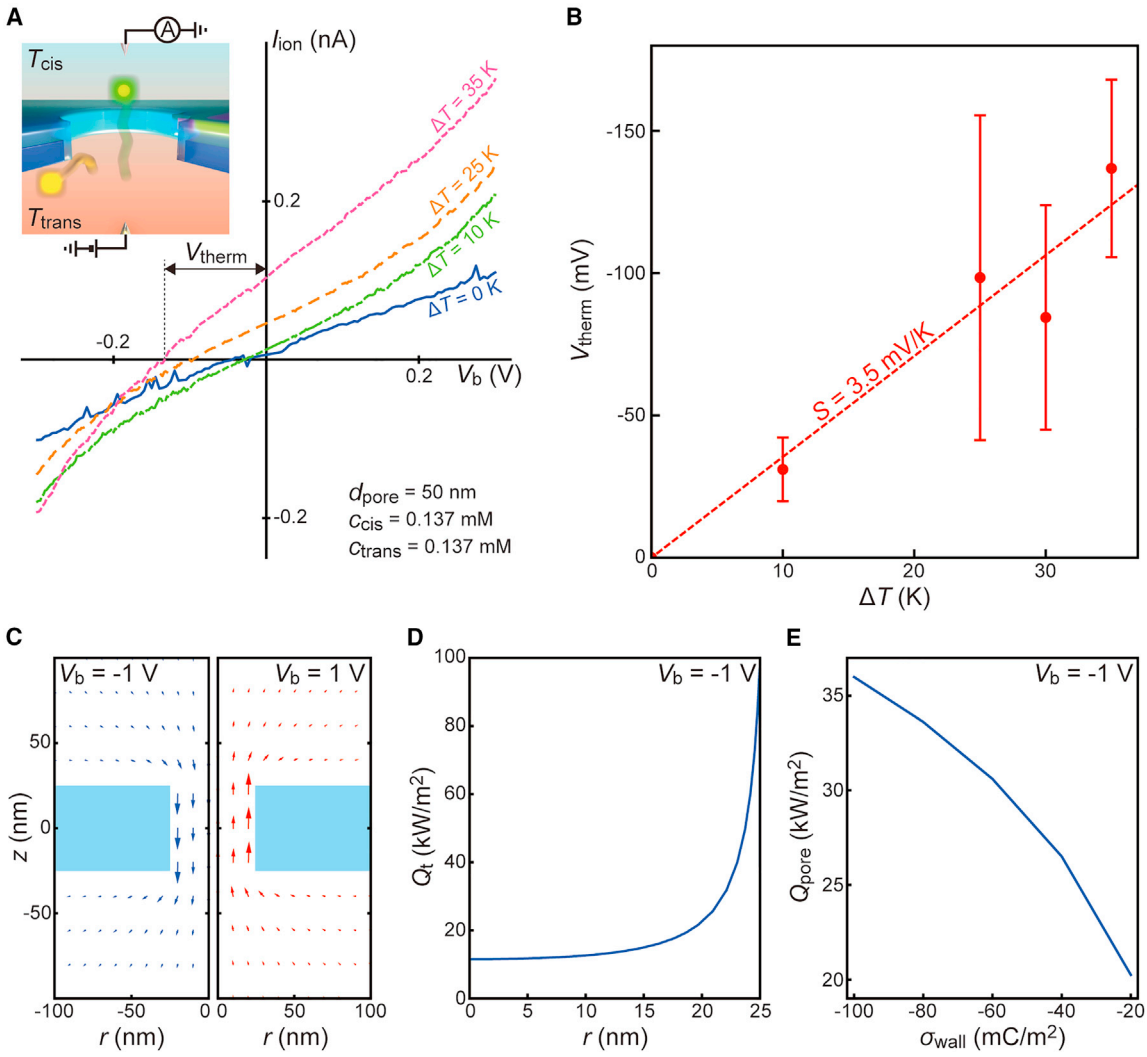

Figure 5. Nanopore cooling mechanism

(A) $I_{ion} - V_b$ characteristics of a 50-nm-sized nanopore under transmembrane temperature gradients. The temperature at the *trans* (T_{trans}) was kept at 283 K while that at the *cis* (T_{cis}) was increased to create temperature difference $\Delta T = T_{cis} - T_{trans}$ at the pore. The open circuit voltage V_{therm} describes the thermovoltage induced by the cation-selective thermal diffusion transport in the nanopore under the applied ΔT.

(B) V_{therm} plotted against ΔT. Dashed line is a linear fit giving the Seebeck coefficient S of 3.5 mV/K. Error bars denote the standard deviations of three measurements.

(C) Finite element simulations of the thermoelectric transport in the nanopore with S = 3.5 mV/K assumed for water. The red and blue arrows are the heat flux vectors.

(D) Variation in the Peltier effect-derived heat flux Q_t inside the nanopore. Q_t is larger near the wall surface manifesting the major contribution of the counter-cation flow on the nanopore cooling.

(E) The average heat flux Q_{pore} in the nanopore plotted as a function of the pore wall surface charge density σ_{wall}. Larger surface charge densities bring stronger counter-cation flows that enable more significant Peltier effects to cool down the nanopore.

counterion flow. In this regard, low length-to-diameter aspect-ratio nanochannels such as 2D nanopores[37] are anticipated to be a promising system that can provide enhanced ion permeabilities, and hence more efficient heat transfer by counterion flows, let alone the ambiguous contribution of the access resistance on the ionic thermoelectricity.

Potential applications for nanofluidic cooling

Beside the structure of channels, surface engineering may also be useful to tailor the membrane surface charge density through molecular functionalization and dielectric coatings[38] to tune the permselectivity[39] for better ionic control of the nanopore temperature. Solution properties can also be arranged by mixing organic solvents, for instance, to reduce the heat capacity.[4]

Since the selective ion transport is the only prerequisite, the nanofluidic cooling is expected to take place in various forms. Nanopore diodes and transistors, for example, can regulate the ionic current via voltage control of charge-selective ion transport through asymmetric channels.[40,41] By exploiting the Peltier effect, one may design devices that can self-cool, such as for

Please cite this article in press as: Tsutsui et al., Peltier cooling for thermal management in nanofluidic devices, Device (2023), https://doi.org/10.1016/j.device.2023.100188

managing the heat dissipation in the integrated iontronic circuits.[42,43]

Solid-state nanopore sequencing is another potential application,[44] where the local ionic cooling can serve to slow down the translocation dynamics of nucleotide and peptide chains for reliable single-base detections via the increased local viscosity,[45] as well as the thermophoretic forces.[46] For these applications, one should consider the low ionic strength requirement for exploiting the thermoelectric phenomenon that would limit the signal-to-noise ratio when used for the single-molecule analyses by the ionic current. The ionic cooling method is thus more compatible with the electrode-embedded nanopore approaches,[47,48] where one can even benefit from the low ion concentration conditions to reduce noise in the transverse electric current.

Nanoporous membrane osmotic power generators exploit the ion selectivity to generate electricity from the transmembrane salinity difference.[49,50] The involved diffusion-driven migration of cations or anions may cause a substantial change in nanopore temperature to the osmotic energy conversion efficiency via the heat pumping mechanism considering the large power densities with the high porosity designs. Alternatively, the local temperature control can be utilized in the multipore reactors for controlling the translocation motions of reactants to in-pore chemical reaction kinetics.[51,52]

It is also noticeable that similar systems exist in biological membranes known as ion channels, where the present findings suggest a possible role of the permselective transmembrane ion flow to regulate the local temperature in a cell.

EXPERIMENTAL PROCEDURES

Resource availability

Lead contact

Further information and requests for resources should be directed to and will be fulfilled by the Lead Contact, Makusu Tsutsui (tsutsui@sanken.osaka-u.ac.jp).

Materials availability

This study did not generate new unique reagents.

Data and code availability

This study did not generate any datasets.

Methods

Thermocouple-embedded nanopore fabrications

AZ5206 photoresist (MicroChemicals) was spin-coated on a 4-inch silicon wafer (both sides of the mirror-finished surfaces coated with low-pressure chemical vapor deposition-grown SiN_x layers of 30 nm thickness). After baking, electrode patterns were delineated by photolithography (Samco). After development, a 20-nm-thick Au film with a 5-nm-thick Cr adhesion layer was deposited by radio-frequency magnetron sputtering (Samco). The wafer was then immersed in *N*,*N*-dimethylformamide (Wako) overnight followed by ultrasonication for lift-off. As a result, we obtained microelectrodes in 9 regions of 20 mm × 20 mm area. Subsequently, the wafer was diced into 25 mm × 25 mm chips by a dicer. On each chip, ZEP520A resist was spin-coated and heated on a hot plate for baking. Cross-shaped Au markers of nanoscale sizes were formed by electron-beam lithography (125 kV, Elionix) followed by the Ti/Au sputtering and lift-off processes. Using these metallic markers, the electron beam lithography process was repeated to delineate a hole of diameter 70 nm at a specific position. After development, a 70-nm-sized nanopore was sculpted by reactive ion etching with HCF_3 etchant gas (Samco) via the residual resist serving as a mask. The lithography/sputtering processes were further performed twice to form a point contact of Au and Pt nanowires at 5 nm from the edge of the nanopore (used as a thermocouple to measure the nanopore temperature), where the markers were used to align the structures at a precision better than 5 nm. The whole structure was then covered with 50-nm-thick Cr by sputtering. The SiN_x layer on the other side was partially removed by reactive ion etching through a 10 mm × 10 mm window in an aluminum film. The exposed Si surface was exposed to heated 20% KOH aq. For anisotropic wet etching that created a deep trench with a 40-nm-thick SiN_x membrane at the bottom. During wet etching, the Cr layer served to protect the nanopore as well as the thermocouple. After rinsing in hot distilled water, the chip was dipped in an etchant solution consisting of tetra ammonium cerium(IV) sulfate dihydrate, perchloric acid (Aldrich), and distilled water to dissolve the Cr layer. Finally, the thermocouple and the nanopore were coated with 20-nm-thick SiO_2 by chemical vapor deposition, which shrunk the pore diameter by approximately 20 nm. Through these processes, we acquired a 50-nm-sized nanopore with an embedded Au/Pt thermocouple.

Flow cell preparations

SU-8 3000 photoresist (MicroChem) was spin-coated on a 4-inch Si wafer with thermally grown oxide layers. Millimeter-scale patterns were drawn by photolithography. After development, we obtained I-shaped SU-8 structures. Using the SU-8-pattered Si wafer as a mold, we prepared fluidic channels for pouring the electrolyte buffers into the thermocouple-embedded nanopores. This was done by pouring Sylgard 184 (Dow) on the mold and heating it in an oven at 90°C for 10 h. The polydimethylsiloxane (PDMS) on the mold was cut by hand with a surgical knife. Prior to bonding to the nanopore chip, three holes were punched in the PDMS block. The bonding was carried out by treating its surface, together with the nanopore chip, with oxygen plasma for surface activation. The activated surface was attached to each other for strong adhesion of the polymeric block to the SiN_x surface. These processes were repeated to bond another PDMS flow cell to the other side of the nanopore chip.

Simultaneous measurements of ionic current and nanopore temperature

The flow cell-integrated thermocouple-nanopore chip was mounted on a sample stage. Metal rods were contacted to the electrode pads connected to the Au/Pt thermocouple. PBS (Wako) of specific ion concentrations was poured into the nanopore through the holes in the PDMS blocks. Ag/AgCl rods were inserted into one of the three holes in each flow cell. The transmembrane ionic current measurements were performed by applying the voltage V_b through one of the Ag/AgCl and recording the output current via the Ag/AgCl at the other side using a source-picoammeter unit (Keithley6487, Keithley). At the same time, the thermovoltage at the thermocouple was measured through the electrode pads using a nanovoltmeter (Keithley2182A, Keithley).

Thermocouple calibrations

The thermocouple was calibrated by heating the structure with an external heater and measuring the voltage change with the nanovoltmeter. The temperature dependence of the thermocouple voltage V_t gave the expression of $T_{pore} = 5.9 \times 10^6 V_t$ as reported in previous literature.[4]

Finite element analyses

Theoretical estimations of the spatial temperature distributions around a nanopore were performed by solving Poisson-Nernst-Planck, Navier-Stokes, and heat equations in a framework of a finite element method. The temperature dependence of the electrolyte buffer was obtained experimentally, from which we calculated the ion mobilities. Nernst-Planck equation,

$$\nabla\cdot\left(-\frac{u_{a,c}k_BT}{e}\nabla n_{a,c} - z_{a,c}n_{a,c}eu_{a,c}\nabla\phi\right) + u\cdot\nabla n_{a,c} = 0$$

was used to estimate the number density distribution of anions n_a and cations n_c, where k_B, e, $z_{a,c}$, and ϕ are the Boltzmann constant (1.38×10^{-23} J/K), elementary charge (1.60×10^{-19} C), ionic valence, and electrostatic potential, respectively. Φ was obtained from the Poisson-Boltzmann equation,

$$\nabla^2\phi = -\frac{\rho_Q}{\varepsilon_w} = -\frac{e}{\varepsilon_w}\sum_{a,c} z_{a,c}n_{a,c}\exp\left(-\frac{z_{a,c}e\phi}{k_BT}\right)$$

where ρ_Q and ε_w are electric charge density and water permittivity. The heat convection induced by the electroosmotic flow from the force $\rho_Q E$ was

simulated by the incompressible Navier-Stokes equation for hydrodynamic pressure p and fluid velocity field u

$$-\nabla \boldsymbol{p} + \eta \nabla^2 \boldsymbol{u} + \rho_Q \boldsymbol{E} = \boldsymbol{0}.$$

Meanwhile, the steady-state heat flow in solids is expressed as

$$\nabla \cdot (\kappa \nabla \boldsymbol{T}) + \boldsymbol{J} \cdot \boldsymbol{E} = \boldsymbol{0},$$

while that in liquids is given as

$$\nabla \cdot (\kappa \nabla \boldsymbol{T}) + \boldsymbol{J} \cdot \boldsymbol{E} = \rho_d \boldsymbol{C_p u} \cdot \nabla \boldsymbol{T},$$

with J, E, κ, T, ρ_d, C_p, and u denoting, respectively, the current density, applied electric field, thermal conductivity, temperature, density, heat capacity, and fluid velocity field. The current density in these equations was coupled to the continuity equation

$$\nabla \cdot \boldsymbol{J} = \boldsymbol{0}.$$

These equations were simultaneously solved by using a software package for finite element methods of COMSOL Multiphysics 6.1 (COMSOL, Inc., Stockholm, Sweden).

SUPPLEMENTAL INFORMATION

Supplemental information can be found online at https://doi.org/10.1016/j.device.2023.100188.

ACKNOWLEDGMENTS

A part of this work was supported by the Japan Society for the Promotion of Science (JSPS) KAKENHI (grant no. 22H01926 and 22K04893).

AUTHOR CONTRIBUTIONS

M.T., H.D., and T.K. conceived the overall ideas and planned experiments; M.T. fabricated the nanopore chips and performed the measurements; M.T., W.-L.H., and D.G. analyzed the data; K.Y. carried out the finite element simulations; M.T. and T.K. co-wrote the manuscript.

DECLARATION OF INTERESTS

The authors declare no competing interests.

Received: August 30, 2023
Revised: November 8, 2023
Accepted: November 13, 2023
Published: December 5, 2023

REFERENCES

1. Chen, D.P., Eisenberg, R.S., Jerome, J.W., and Shu, C.-W. (1995). Hydrodynamic model of temperature change in open i onic channels. Biophys. J. *69*, 2304–2322.
2. Nagashima, G., Levine, E.V., Hoogerheide, D.P., Burns, M.M., and Golovchenko, J.A. (2014). Superheating and homogeneous single bubble nucleation in a solid-state nanopore. Phys. Rev. Lett. *113*, 024506.
3. Paul, S., Hsu, W.-L., Ito, Y., and Daiguji, H. (2022). Boiling in nanopores through localized Joule heating: transition between nucleate and film boiling. Phys. Rev. Res. *4*, 043110.
4. Tsutsui, M., Arima, A., Yokota, K., Baba, Y., and Kawai, T. (2022). Ionic heat dissipation in solid-state pores. Sci. Adv. *8*, abl7002.
5. Bernges, T., Hanus, R., Wankmiller, B., Imasato, K., Lin, S., Ghidiu, M., Gerlitz, M., Peterlechner, M., Graham, S., Hautier, G., et al. (2022). Considering the role of ion transport in diffusion-dominated thermal conductivity. Adv. Energy Mater. *12*, 2200717.
6. Sun, S., Li, M., Shi, X.-L., and Chen, Z.-G. (2023). Advances in ionic thermoelectrics: from materials to devices. Adv. Energy Mater. *13*, 2203692.
7. Vlassiouk, I., Smirnov, S., and Siwy, Z. (2008). Ionic selectivity of single nanochannels. Nano Lett. *8*, 1978–1985.
8. Faucher, S., Aluru, N., Bazant, M.Z., Blankschtein, D., Brozena, A.H., Cumings, J., Pedro de Souza, J., Elimelech, M., Epsztein, R., Fourkas, J.T., et al. (2019). Critical knowledge gaps in mass transport through single-digit nanopores: a review and perspective. J. Phys. Chem. C *123*, 21309–21326.
9. Catterall, W.A. (1995). Structure and function of voltage-gated ion channels. Annu. Rev. Biochem. *64*, 493–531.
10. Clapham, D.E., Runnels, L.W., and Strübing, C. (2001). The TRP channel family. Nat. Rev. Neurosci. *2*, 387–396.
11. Rollings, R.C., Kuan, A.T., and Golovchenko, J.A. (2016). Ion selectivity of graphene nanopores. Nat. Commun. *7*, 11408.
12. Chen, K., Yao, L., and Su, B. (2019). Bionic thermoelectric response with nanochannels. J. Am. Chem. Soc. *141*, 8608–8615.
13. Vriens, J., Nilius, B., and Voets, T. (2014). Peripheral thermosensation in mammals. Nat. Rev. Neurosci. *15*, 573–589.
14. Song, D., Li, L., Huang, C., and Wang, K. (2023). Synergy between ionic thermoelectric conversion and nanofluidic reverse electrodialysis for high power density generation. Appl. Energy *334*, 120681.
15. Nolas, G.S., Sharp, J., and Goldsmid, H.J. (2001). Thermoelectrics: Basic principles and new materials developments. Springer Series in Materials Science (Springer).
16. Garaj, S., Hubbard, W., Reina, A., Kong, J., Branton, D., and Golovchenko, J.A. (2010). Graphene as a subnanometre trans-electrode membrane. Nature *467*, 190–193.
17. Israelachvili, J. (2003). Intermolecular and Surface Forces, 2nd ed. (Academic Press).
18. Welty, J.R., Wicks, C.E., Wilson, R.E., and Rorrer, G. (2001). Fundamentals of Momentum, Heat, and Mass Transfer (Wiley).
19. Menzel, R., Barg, S., Miranda, M., Anthony, D.B., Bawaked, S.M., Mokhtar, M., Al-Thabaiti, S.A., Basahel, S.N., Saiz, E., and Shaffer, M.S.P. (2015). Joule heating characteristics of emulsion-templated graphene aerogels. Adv. Funct. Mater. *25*, 28–35.
20. Cheng, L.-J., and Guo, L.J. (2010). Nanofluidic diodes. Chem. Soc. Rev. *39*, 923–938.
21. Yusko, E.C., An, R., and Mayer, M. (2010). Electroosmotic flow can generate ion current rectification in nano- and micropores. ACS Nano *4*, 477–487.
22. Cheng, L.J., and Guo, L.J. (2007). Rectified ion transport through concentration gradient in homogeneous silica nanochannels. Nano Lett. *7*, 3165–3171.
23. Kim, D.-K., Duan, C., Chen, Y.-F., and Majumdar, A. (2010). Power generation from concentration gradient by reverse electrodialysis in ion-selective nanochannels. Microfluid. Nanofluidics *9*, 1215–1224.
24. van Dorp, S., Keyser, U.F., Dekker, N.H., Dekker, C., and Lemay, S.G. (2009). Origin of the electrophoretic force on DNA in solid-state nanopores. Nat. Phys. *5*, 347–351.
25. Lee, C., Joly, L., Siria, A., Biance, A.-L., Fulcrand, R., and Bocquet, L. (2012). Large apparent electric size of solid-state nanopores due to spatially extended surface conduction. Nano Lett. *12*, 4037–4044.
26. Tang, W., Fried, J.P., Tilley, R.D., and Gooding, J.J. (2022). Understanding and modelling the magnitude of the change in current of nanopore sensors. Chem. Soc. Rev. *51*, 5757–5776.
27. Li, C.-Y., Ma, F.-X., Wu, Z.-Q., Gao, H.-L., Shao, W.-T., Wang, K., and Xia, X.-H. (2013). Solution-pH-modulated rectification of ionic current in highly ordered nanochannel arrays patterned with chemical functional groups at designed positions. Adv. Funct. Mater. *23*, 3836–3844.
28. Tsutsui, M., Yokota, K., Leong, I.-W., He, Y., and Kawai, T. (2022). Sparse multi-nanopore osmotic power generators. Cell Rep. Phys. Sci. *3*, 101065.

29. Chen, W.Q., Sedighi, M., and Jivkov, A.P. (2022). Thermal diffusion of ionic species in charged nanochannels. Nanoscale *15*, 215–229.

30. Quickenden, T.I., and Mua, Y. (1995). A review of power generation in aqueous thermogalvanic cells. J. Electrochem. Soc. *142*, 3985–3994.

31. Fu, L., Joly, L., and Merabia, S. (2019). Giant thermoelectric response of nanofluidic systems driven by water excess enthalpy. Phys. Rev. Lett. *123*, 138001.

32. Jin, Y., Tao, R., Luo, S., and Li, Z. (2021). Size-sensitive thermoelectric properties of electrolyte-based nanofluidic systems. J. Phys. Chem. Lett. *12*, 1144–1149.

33. Lu, C., Hu, C., Ritt, C.L., Hua, X., Sun, J., Xia, H., Liu, Y., Li, D.-W., Ma, B., Elimelech, M., and Qu, J. (2021). *In situ* characterization of dehydration during ion transport in polymeric nanochannels. J. Am. Chem. Soc. *143*, 14242–14252.

34. Qiao, R., and Aluru, N.R. (2005). Atomistic simulation of KCl transport in charged silicon nanochannels: Interfacial effects. Colloids Surf., A *267*, 103–109.

35. Shi, Y., and Beck, T.L. (2020). Absolute ion hydration free energy scale and the surface potential of water via quantum simulation. Proc. Natl. Acad. Sci. USA *117*, 30151–30158.

36. Cao, L., Wen, Q., Feng, Y., Ji, D., Li, H., Li, N., Jiang, L., and Guo, W. (2018). On the origin of ion selectivity in ultrathin nanopores: Insights for membrane-scale osmotic energy conversion. Adv. Funct. Mater. *28*, 1804189.

37. Macha, M., Marion, S., Nandigana, V.V.R., and Radenovic, A. (2019). 2D materials as an emerging platform for nanopore-based power generation. Nat. Rev. Mater. *4*, 588–605.

38. Eggenberger, O.M., Ying, C., and Mayer, M. (2019). Surface coatings for solid-state nanopores. Nanoscale *11*, 19636–19657.

39. Ji, J., Kang, Q., Zhou, Y., Feng, Y., Chen, X., Yuan, J., Guo, W., Wei, Y., and Jiang, L. (2016). Osmotic power generation with positively and negatively charged 2D nanofluidic membrane pairs. Adv. Funct. Mater. *27*, 1603623.

40. Wu, R., Hao, J., Cui, Y., Zhou, J., Zhao, D., Zhang, S., Wang, J., Zhou, Y., and Jiang, L. (2023). Multi-control of ion transport in a field-effect iontronic device based on sandwich-structured nanochannels. Adv. Funct. Mater. *33*, 2208095.

41. Hu, Y.-L., Hua, Y., Pan, Z.-Q., Qian, J.-H., Yu, X.-Y., Bao, N., Huo, X.-L., Wu, Z.-Q., and Xia, X.-H. (2022). PNP nanofluidic transistor with actively tunable current response and ionic signal amplification. Nano Lett. *22*, 3678–3684.

42. Li, J., Li, M., Zhang, K., Hu, L., and Li, D. (2023). High-performance integrated iontronic circuits based on single nano/microchannels. Small *19*, 2208079.

43. Zhang, E., Galle, L., Lochmann, S., Grothe, J., and Kaskel, S. (2021). Nanoporous carbon architectures for iontronics: ion-based computing, logic circuits and biointerfacing. Chem. Eng. J. *420*, 130431.

44. Xue, L., Yamazaki, H., Ren, R., Wanunu, M., Ivanov, A.P., and Edel, J.B. (2020). Solid-state nanopore sensors. Nat. Rev. Mater. *5*, 931–951.

45. Fologea, D., Uplinger, J., Thomas, B., McNabb, D.S., and Li, J. (2005). Slowing DNA translocation in a solid-state nanopore. Nano Lett. *5*, 1734–1737.

46. Zhang, M., Ngampeerapong, C., Redin, D., Ahmadian, A., Sychugov, I., and Linnros, J. (2018). Thermophoresis-controlled size-dependent DNA translocation through an array of nanopores. ACS Nano *12*, 4574–4582.

47. Tang, L., Nadappuram, B.P., Cadinu, P., Zhao, Z., Xue, L., Yi, L., Ren, R., Wang, J., Ivanov, A.P., and Edel, J.B. (2021). Combined quantum tunnelling and dielectrophoretic trapping for molecular analysis at ultra-low analyte concentrations. Nat. Commun. *12*, 913.

48. Heerema, S.J., Vicarelli, L., Pud, S., Schouten, R.N., Zandbergen, H.W., and Dekker, C. (2018). Probing DNA translocations with inplane current signals in a graphene nanoribbon with a nanopore. ACS Nano *12*, 2623–2633.

49. Zhang, Z., Wen, L., and Jiang, L. (2021). Nanofluidics for osmotic energy conversion. Nat. Rev. Mater. *6*, 622–639.

50. Yang, J., Tu, B., Zhang, G., Liu, P., Hu, K., Wang, J., Yan, Z., Huang, Z., Fang, M., Hou, J., et al. (2022). Advancing osmotic power generation by covalent organic framework monolayer. Nat. Nanotechnol. *17*, 622–628.

51. Venta, K., Wanunu, M., and Drndić, M. (2013). Electrically controlled nanoparticle synthesis inside nanopores. Nano Lett. *13*, 423–429.

52. Wood, M., and Zhang, B. (2015). Bipolar electrochemical method for dynamic in situ control of single metal nanowire growth. ACS Nano *9*, 2454–2464.